International Journal of Thermal Sciences 49 (2010) 664–674

Contents lists available at ScienceDirect

International Journal of Thermal Sciences

journal homepage: www.elsevier.com/locate/ijts

A new database on the evolution of air–water flows along a large vertical pipe

D. Lucas*, M. Beyer, L. Szalinski, P. Schütz

Forschungszentrum Dresden-Rossendorf e.V., Institute of Safety Research, P.O. Box 510 119, 01314 Dresden, Germany

ARTICLE INFO

Article history:
Received 15 April 2009
Received in revised form
6 November 2009
Accepted 9 November 2009
Available online 5 December 2009

Keywords:
Multiphase flow
Bubbly flow
Churn turbulent flow
Annular flow
Bubble size
Pipe flow

ABSTRACT

A comprehensive database was obtained for stationary upward air–water flows in a vertical pipe with an inner diameter of 195.3 mm using the wire-mesh sensor technology. During the experiments the sensor was always mounted on the top of the test section while the distance between gas injection and measuring plane was varied to up to 18 different L/D by using gas injection chambers at different vertical positions. The gas was injected via holes in the pipe wall. The pressure was kept at 0.25 MPa (absolute) at the location of the active gas injection while the temperature was constant at 30 °C ± 1 K. This procedure exactly represents the evolution of the flow along the pipe, as it would be observed for an injection at a constant height position and a shifting of the measurement plane. The experiments were done for 48 combinations of air and water superficial velocities varying from 0.04 m/s to 1.6 m/s for water and 0.0025 m/s to 3.2 m/s for air. From the raw data time-averaged data as: radial gas volume fraction profiles, bubble size distributions, radial volume fraction profiles decomposed according to the bubble size and the radial profiles of the gas velocity were calculated. Due to the combination of the new experimental procedure with the high spatial and temporal resolution of the wire-mesh sensor technology the data have new quality especially regarding their consistency in the evolution with increasing L/D. This closes a gap for data suitable for CFD code development and validation for two-phase flows, especially for models on bubble coalescence and break-up.

1. Introduction

Two-phase flows occur in many applications in chemical and petrochemical industries. For design, process optimization and safety analyses the physics of these flows have to be well understood and models on different levels of detailedness are required. Gas–liquid flow in vertical pipes is a very good subject for studying the corresponding phenomena. Here, bubbles or large gas structures move under well known boundary conditions for a comparatively long time. This allows e.g. studying the lateral motion of the bubbles in shear flows which is connected with lateral bubble forces but also phenomena as bubble coalescence and break-up by comparing radial gas distributions and/or bubble size distributions measured at different distances from the gas injection.

Also, the use of Computational Fluid Dynamics (CFD) codes for simulations of two-phase flow phenomena comes more and more into the focus of multiphase flow research. This requires the qualification of the basic model concepts as well as closure models, since such applications are not mature. The qualification procedure includes model development, test and validation. Especially in case of poly-dispersed flows there are still many open questions which have to be answered. Thus e.g. the presently available models for bubble coalescence and break-up are weak and can predict the evolution of the flow only for a narrow range of flow conditions [5]. Experimental data with high resolution in space and time are required for the model improvement [7,8].

The aim of the experiments presented in this paper was to establish a high-quality database on the evolution of upwards air–water flows in a vertical pipe with a nominal diameter of 200 mm containing detailed information on two-phase flow characteristics. This includes different flow pattern as bubbly flow, churn turbulent flow and wispy annular flow. Based on the experiences gained from previous experimental series [6,19,20], continuous high quality and consistency of the data have been basic requirements for these tests.

All the measuring techniques which are presently available for measurements with high resolution in space and time in flows with high gas volume fraction have an influence on the flow downstream the measuring position (most of them base on needle probes of different types, see e.g. [10]). For this reason the facilities have to be reassembled in case of measurements for different L/D to shift the measuring technique. The single measurements for a given set of boundary conditions, but varying L/D cannot be done directly one after the other. Instead the information on the evolution of the

* Corresponding author. Tel.: +49 351 260 2047; fax: +49 351 260 12047.
E-mail address: D.Lucas@fzd.de (D. Lucas).

1290-0729/$ – see front matter © 2009 Elsevier Masson SAS. All rights reserved.
doi:10.1016/j.ijthermalsci.2009.11.008

flow is obtained from separate experimental runs. The experience with such experiments clearly showed, that this leads to additional discrepancies in the data like bubble size distributions which are very sensitive regarding boundary conditions and especially regarding fluid properties.

For this reason and because of the problems to reassemble a large facility the so-called variable gas injection device was recently developed and operated successfully at Forschungszentrum Dresden-Rossendorf. For these experiments the measurement plane is located always at the upper end of the pipe while gas is injected via orifices in the tube wall in different distances of this measurement plane. This allows to conduct experiments on the evolution of the flow with increasing L/D without reassembling the facility to shift the measuring plane, but just by switching between devices used for the gas injection. A disadvantage of the previous experiments using the variable gas injection, described in detail by Prasser et al. [19,20], was that the pressure at the individual positions of the gas injection varied due to the hydrostatic pressure, because the pressure was almost constant at the measurement plane. In contrast to these previous test series, the measurements were now accomplished in such a way that they reflect the evolution of the two-phase flow along the pipe under constant conditions for the gas injection. Also the new database has a considerably improved quality thanks to an improved water temperature control, the extended test matrix and much higher consistency of the data.

CFD simulations for the evolution of poly-disperse bubbly flows have particularly shown that the models of bubbly coalescence and fragmentation must be further optimised [7,5]. At relatively small void fractions, the pressure effect on the increase in bubble size can have a larger influence on the evolution of the bubble size distribution than coalescence and fragmentation. Prasser et al. [20] discuss which essentially influence the bubble expansion may have on the bubble size distribution basing on experimental and numerical results.

Therefore, in the test series presented in this paper the pressure was kept constant at the respective gas injection. The measurement data represent the evolution of the flow along the pipe, as it would be observed for an injection at a constant height position with an associated shift of the measurement plane. All measurements were performed at a nearly constant temperature of $T = 30$ °C. The deviations were smaller than 1 K. This is important because the coalescence rate and break-up frequency sensitively depend on the temperature caused by the effect of the surface tension.

Extensive cross-checks of the plausibility of the data against each other were done. This concerns the consistent evolution of time-averaged profiles and the bubble size distribution with increasing height scale L/D as well as the comparison of the gas volume flow obtained from measurement data with the setting data. This enables a global error assessment and shows the dependence of the accuracy of the measurements on the respective flow conditions. The time and cross-section averaged gas volume fraction values are compared to those obtained from drift models considering profiles effects and effects of varying bubble rise velocities with varying bubble sizes.

There are a large number of publications regarding measurements on two-phase flow within vertical pipes of different diameters (e.g. [22,2,3,12,26,24,11,6,23,20]). However the database presented in this paper is unique regarding their detailed information on important two-phase flow parameter, regarding the spatial and temporal resolution of the data and regarding the quality. Since a large number of measuring points are in the region of bubbly flow it is especially, but not only, suitable for model development and validation for poly-dispersed flows. The clear trends in the evolution of the flow with increasing L/D qualifies the data e.g. for the development and validation of models for bubble coalescence and break-up. The experiments, measuring technique, calibration and data evaluation procedures, error assessment and experimental results are documented in detail in an experiment report by Beyer et al. [1].

2. Description of the experiments

2.1. TOPFLOW-test section "variable gas injection"

The measurements were carried out at the **T**ransient tw**O-P**hase **FLOW** test facility (TOPFLOW) of the Institute of Safety Research at the Forschungszentrum Dresden-Rossendorf. The facility is described in detail by Schaffrath et al. [21] and Prasser et al. [18]. One of the installed test sections is the so-called variable gas injection (see Fig. 1), which consists of a vertical steel pipe with an inner diameter of 195.3 mm and a length of about 8 m. It is equipped with six gas injection units which allow to inject air or steam via orifices in the pipe wall. They are arranged almost logarithmically over the pipe length. Each module (Fig. 2) consists of three chambers. This gas injection via wall orifices offers the advantage that the two-phase flow can rise smoothly to the measurement plane, without being influenced by the feeder within the tube in other height positions. Two of the three chambers (the uppermost and the lowest) have 72 × 1 mm orifices. The middle chamber has 32 × 4 mm orifices, which is used to vary the initial bubble size distribution. For rotation-symmetric gas injection, all orifices per chambers are equally distributed over the circumference of the pipe.

The chambers can be operated separately and are connected with a gas injection pipe and the compressed air system (Fig. 1). The supply of the liquid phase is done from the bottom of the test section by means of an isolating valve and a 90° bend. During the experiments, a module for central gas injection has been mounted at the lower end of the test section. However, it was not employed in this test series. As a result of the large distance to the measurement plane, the influence of this component on the measured flow properties can be neglected.

The measurement plane was always situated at the upper end of the test section (Fig. 1). A wire-mesh sensor with two measuring planes was used. Table 1 lists the vertical distances between the individual gas injections and the first measurement plane of the wire-mesh sensor located in direction of flow. To use the data for the validation of CFD models, the data obtained at the smallest distance between gas injection and measuring plane (i.e. at $L/D = 1.1$ for injection via 1 mm orifices and at $L/D = 1.4$ for 4 mm orifices) can be used as boundary conditions. Starting from this level the evolution of the flow can be simulated and compared to the experimental data at the corresponding height positions.

2.2. Measuring technique

Measurements were done using wire-mesh sensors. Numerous publications were published in the past on the wire-mesh sensor technology (e.g. [13,15]) and on experiments using the wire-mesh sensor (e.g. [16,20,6,7]). One measuring plane of the sensor consists of two grids of parallel wires, which span over the measurement cross-section. The wires of both planes cross under an angle of 90°, but do not touch. Instead there is a vertical distance between the wires at the crossing points. At these points the conductivity is measured. According to the different conductivity of air and water the phase present in the moment of the measurement at the crossing point can be determined. Many different types of wire-mesh sensors including such for an operational pressure up to 7 MPa and temperatures up to 290 °C were built and successfully

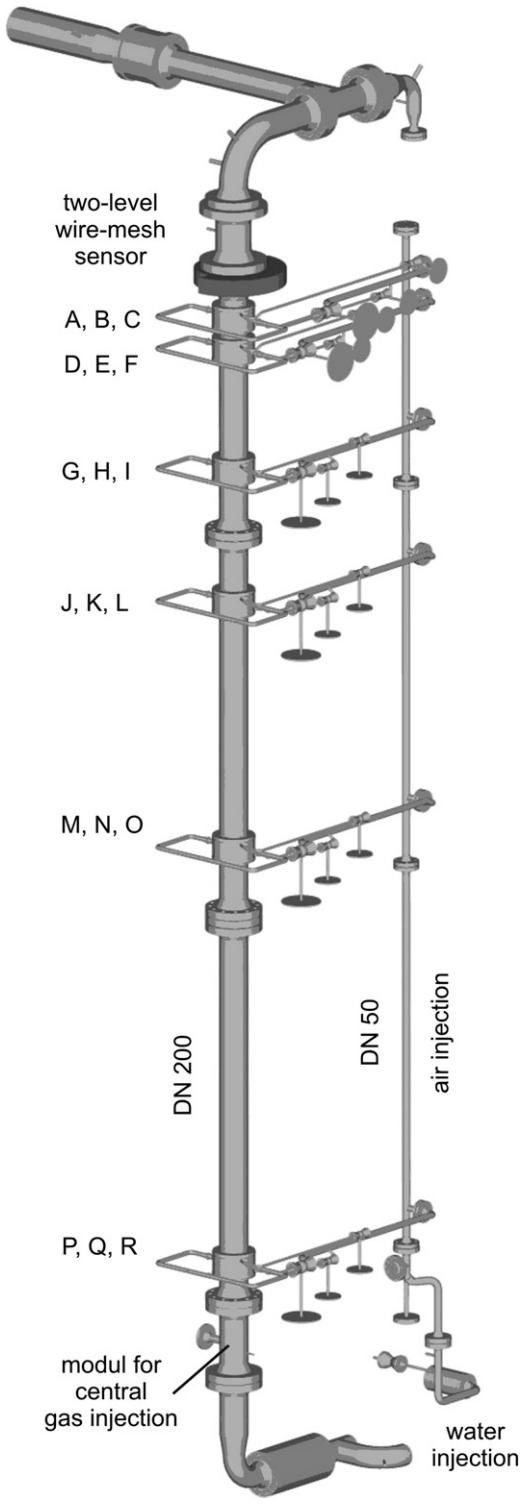

Fig. 1. Scheme of the vertical test section of the TOPFLOW facility with variable gas injection system (DN 200).

used during the last 15 years. Also recent developments which allow measuring the capacity extent the field of applications to non-conducting fluids like oil–nitrogen flows.

In the present case, a low temperature wire-mesh sensor with two measuring planes was employed. Each plane is composed of 64 × 64 wires. It consists of two printed circuit boards (material thickness: 2.5 mm). Both of them are equipped with pre-stressed

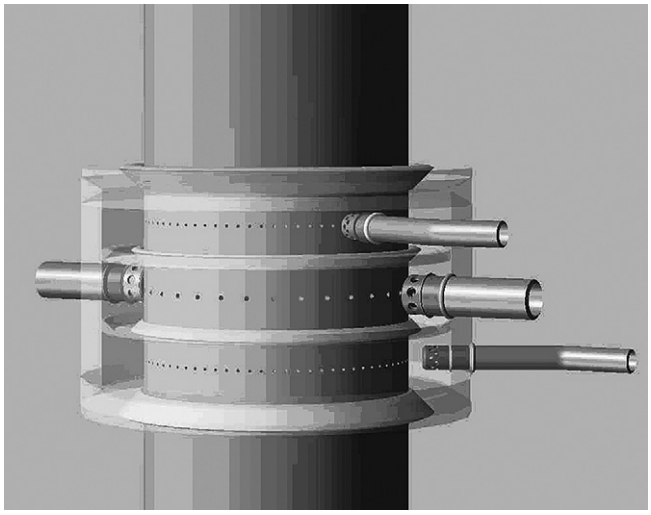

Fig. 2. Injection module of the variable gas injection.

wire electrodes being soldered at a 90° angle to each other on the upper and lower surface. The wires have a lateral distance of 3 mm. In order to make the mechanical sealing of the sensor possible, the wire electrodes with a diameter of 0.125 mm were mounted in approx. 0.3 mm deeply in-milled slots on the printed circuit board. As a result of this construction form, the distance between the two grid levels arises to approx. 2 mm.

The prepared printed circuit boards are installed between two flanges and the intermediate ring (see Fig. 3). The distance of 40.5 mm between both printed circuit boards, and thus between the measurement planes results from the thickness of the intermediate ring, as well as from the pressed silicone seals. In order to reduce the weight of the sensor, the intermediate ring is partially made of aluminium. Four plastic spacer rings are used in the sensor, in order to limit the contact pressure on the silicone sealing rings and, in the case of a repeated assembling, to ensure a reproducible distance of the planes of measurement. It is important to mention, that the downstream measuring plane is only used for the determination of the gas velocity using a cross-correlation methods. Radial profiles and bubble size distribution are determined only from the upstream measuring plane since at the second plane these properties are disturbed due to the first plane.

Table 1
Denotation and positions of the gas injection chambers.

Injection device	Denotation	Diameter of the inlet orifice [mm]	Injection length [mm]	*L*/*D* ratio
1	A	1	221	1.1
1	B	4	278	1.4
1	C	1	335	1.7
2	D	1	494	2.5
2	E	4	551	2.8
2	F	1	608	3.1
3	G	1	1438	7.4
3	H	4	1495	7.7
3	I	1	1552	7.9
4	J	1	2481	12.7
4	K	4	2538	13.0
4	L	1	2595	13.3
5	M	1	4417	22.6
5	N	4	4474	22.9
5	O	1	4531	23.2
6	P	1	7688	39.4
6	Q	4	7745	39.7
6	R	1	7802	39.9

Fig. 3. The installed wire-mesh sensor with two measuring planes.

Measurements were done with a frequency of 2500 frames per second, i.e. 2500 pictures of the instantaneous gas distribution in the pipe cross-section are obtained per second. The measuring time was 10 s for each single measurement, i.e. the result of one measurement is a three-dimensional matrix of 64 × 64 × 25.000 values of the instantaneous local conductivity. By a calibration procedure described below a matrix of the instantaneous local volume void fraction with the same dimensions is calculated. Depending on the flow rates between 10.000 and 750.000 bubbles were identified during the 10 s measuring time. This is sufficient to obtain data with small statistical errors for all flow conditions.

2.3. Boundary conditions and measuring matrix

Special attention was paid to the pressure and temperature boundary conditions during these experiments. As stated above the pressure was kept constant at 0.25 MPa (a) at the location of the activated gas injection to represent the situation of an evolutional flow by using the different gas injections. Since a pressure measurement is done only close to the position of the wire-mesh sensor the set pressure at this location has to be determined. This was done considering the hydrostatic pressure and the pressure drop due to friction. The gas volume fraction which is needed for this calculation was determined from the set values of the air and water superficial velocities and the assumption of a constant drift velocity of 0.25 m/s. The validity of this assumption will be discussed in Section 4.1.

A special operational procedure was used to keep the water temperature constant at 30 °C with a maximal deviation of 1 K. Special flow meters were used to minimize the error of the flow rates. Details on the test procedure, calibration values and errors of the operational instrumentation are documented in the experiment report mentioned above.

Table 2 shows the measuring matrix, i.e. the combinations of air and water superficial velocities measured. Two test series were done with constant liquid superficial velocities of 0.405 m/s and 1.017 m/s and increasing gas superficial velocities, respectively.

Table 2
Test matrix: measurements were done for the marked points.

Superficial water velocity J_L [m/s] \ Superficial gas velocity J_G [m/s] (at 0.25 MPa (absolute))	0.0025	0.004	0.0062	0.0096	0.0151	0.0235	0.0368	0.0574	0.0898	0.14	0.219	0.342	0.534	0.835	1.305	2.038	3.185
1.611	009	020	031	042	053	064	075	086	097	108	119	130	141	152	163	174	185
1.017	008	019	030	041	052	063	074	085	096	107	118	129	140	151	162	173	184
0.641	007	018	029	040	051	062	073	084	095	106	117	128	139	150	161	172	183
0.405	006	017	028	039	050	061	072	083	094	105	116	127	138	149	160	171	182
0.255	005	016	027	038	049	060	071	082	093	104	115	126	137	148	159	170	181
0.161	004	015	026	037	048	059	070	081	092	103	114	125	136	147	158	169	180
0.102	003	014	025	036	047	058	069	080	091	102	113	124	135	146	157	168	179
0.0641	002	013	024	035	046	057	068	079	090	101	112	123	134	145	156	167	178
0.0405	001	012	023	034	045	056	067	078	089	100	111	122	133	144	155	166	177
Flow regimes:	bubbly								transition bubbly → churn		churn turbulent			Wispy annular			

In two other series the gas superficial velocities were kept constant (0.0096 m/s and 0.219 m/s at 0.25 MPa (a)) and the liquid superficial velocity was varied. Table 2 also provides the information on the flow regime observed for each measured combination of air and water superficial velocities.

For investigations on the evolution of the flow along the pipe, all levels (A–R) shown in Table 1 and Fig. 1, were measured for any points smaller than 149. The maximum possible gas flow rate, which can be injected through the injection chambers with a diameter of 1 mm, is limited. For this reason for the points 149, 151, 160 and 162 both injection chambers with 1 mm orifices were operated parallel. For the measurement points 171, 173, 182, 184 only the 4 mm injections were used.

3. Results

From the raw data, i.e. the 64 × 64 × 25.000 matrix of voltage signals representing the instantaneous local conductivity a matrix with the same dimensions containing the respective void fraction values are obtained by a calibration procedure. The conductivity of the gas is negligibly small. Two calibration methods are applied – the so-called histogram calibration and the use of calibration files. The latter ones are obtained by measurements for pure water flow from which the pure water signal levels are determined for each crossing point. The disadvantage of this method is that the conductivity of the water may slightly change with time by several causes. For this reason the histogram calibration is preferred which obtains the pure water signal levels directly from the measured data. A histogram of the measured voltage values is generated for each crossing point of the wire-mesh sensor and each single measurement. Usually two peaks are observed in these histograms – one (close to zero) representing the pure gas the other the pure liquid value. The disadvantage of this method is that it fails for flows with very high gas loads where only few values for pure water are available. In a mixed approach the histogram method is used first. The obtained radial profiles for the pure water calibration values are evaluated afterwards. In case they show inconsistencies in the pipe centre (where the void fraction is largest) calibration files are used. Once the calibration values are determined for each matrix point the void fraction values are calculated assuming a linear dependence between voltage values and gas volume fraction.

The 64 × 64 × 25.000 matrix of void fraction values now can be used to obtain relevant data by averaging procedures. By averaging over the pipe cross-section time series of the void fraction are obtained. The according averaging procedure considers the different measuring volumes in the region of the pipe wall by individual weight coefficients for the single meshes. Such data are used e.g. by Kaji et al. [4] to obtain characteristic parameters of the flow like slug frequencies. Most data however are obtained by time averaging, which e.g. leads to time-averaged two-dimensional gas volume fraction distributions in the pipe cross-section.

Due to the radial symmetry of the data the statistical error can be further reduced by an azimuthally averaging. To do this the cross-section is sub-divided into 80 ring-shaped domains with equal radial width. The contribution of each mesh is calculated by weight coefficients obtained from a geometrical assignment of the fractions of a mesh belonging to these rings. In the result radial gas volume fraction profiles are obtained.

Examples of such profiles are shown in Figs. 4–6. The evolution of the profiles with increasing distance between gas injection and measuring plane always shows a clear trend as demonstrated in Fig. 4. The curves are shown only for 6 of 12 measured L/D to keep the clearness of the figure, but also the remaining curves also fit well into this trend. A comparison of radial gas volume fraction profiles for largest L/D depending on the gas volume flow rate is

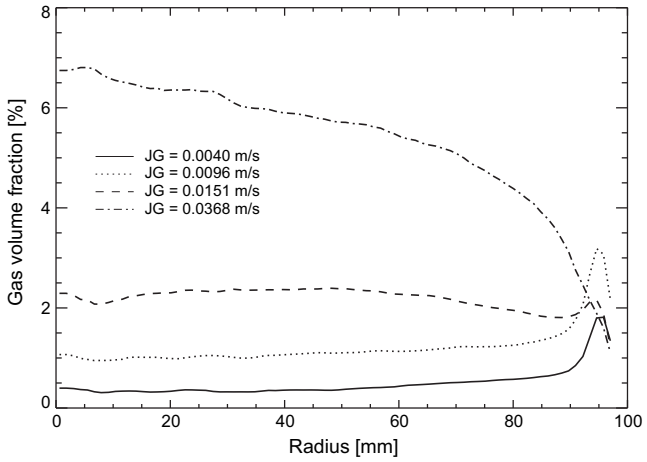

Fig. 5. Example for the dependency of the radial gas volume fraction profiles on the gas superficial velocity J_G. Liquid superficial velocity $J_L = 1.017$ m/s, injection via 1 mm orifices, $L/D = 39.9$.

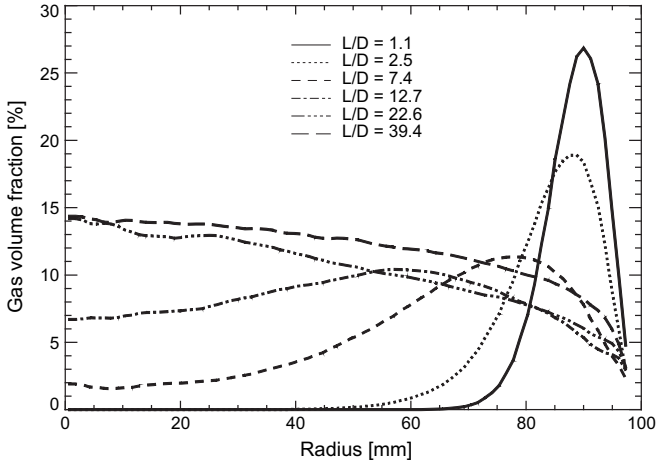

Fig. 4. Example for the evolution of the radial gas volume fraction profile with increasing distance between gas injection and measuring plane. $J_L = 1.017$ m/s, $J_G = 0.0898$ m/s, injection via 1 mm orifices.

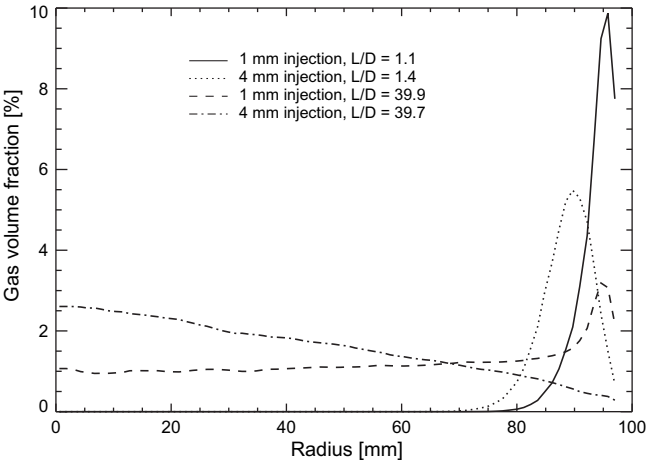

Fig. 6. Example for the dependency of the radial gas volume fraction profiles on the type of injection orifices used. Liquid superficial velocity $J_L = 1.017$ m/s, gas superficial velocity $J_G = 0.0096$ m/s.

given in Fig. 5. While for small flow rates a wall peak is observed, a centre peak occurs for large gas flow rates. This caused by the increase of the averaged bubble size due to coalescence. As discussed e.g. by [8] due to the lateral lift force small bubbles can be found preferred in the near wall region while large bubble migrate towards the centre of the pipe. This effect is also the reason for the measured profiles shown in Fig. 6. Also at the largest L/D measured the profiles clearly differ in case of different initial bubble size distributions resulting from the different injection orifices used.

As mentioned above a sensor with two measuring planes was used. This allows to cross-correlate the gas volume fraction values of the two-planes for all mesh points which are located above each other. From the maxima of the cross-correlation functions the typical time shift of the local void fraction fluctuations can be determined. Since the distance between the measuring planes is known the local time-averaged gas velocity can be calculated. The point-to-point two-dimensional gas velocity distributions in the pipe cross-section are obtained in the results of this procedure. Again an azimuthally averaging is applied to obtain the radial profiles of the gas velocity. Examples for such radial profiles of the gas velocity are given in Figs. 7 and 8. Fig. 7 shows a case with relatively small gas volume fraction resulting in typical velocity profiles which have their maximum in the pipe centre. In the case of high gas volume fraction shown in Fig. 8 for small L/D the maximum velocity is close to the wall. This is caused by secondary flows due to the acceleration of liquid by the injected gas in vertical direction. For small L/D no bubbles are observed in the pipe centre. For this reason no gas velocity can be determined for small radial positions. Also the relatively large fluctuations of the measured gas velocity for small L/D and medium radial positions are caused by the fact, that only very few bubbles were observed in this region.

The next step of the data evaluation procedure is the identification of single bubbles. Thereby, a bubble is defined as a region of connected gas-containing elements in the void fraction matrix which is completely surrounded by elements containing the liquid phase. A complex procedure, described by Prasser et al. [15], applies filling and agglomeration algorithms combined with sophisticated stop criteria to avoid artificial combinations as well as artificial fragmentation of bubbles. In the result to each element which belongs to one bubble, the same identification number is assigned. Different bubbles receive different identification numbers. These numbers are stored in the elements of a second array. This array has the same dimension as the void fraction array. Combining the information from the void faction and bubble number arrays

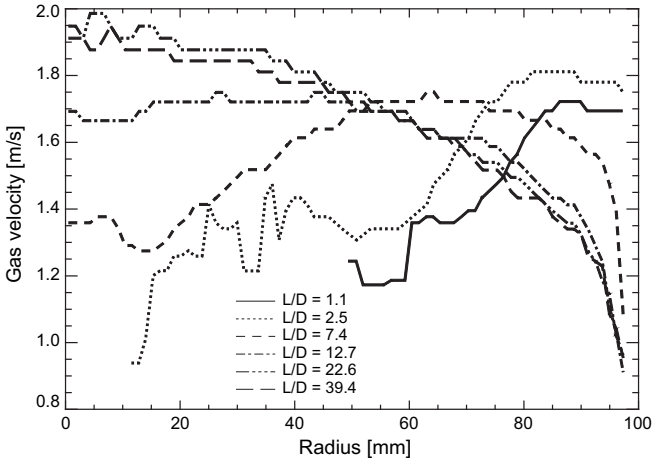

Fig. 8. Example for the evolution of the radial gas velocity profile with increasing distance between gas injection and measuring plane for a high void fraction case. $J_L = 1.017$ m/s, $J_G = 0.140$ m/s, injection via 1 mm orifices.

together with the radial profiles of the gas velocity characteristic data of the single bubbles as bubble volume, sphere equivalent bubble diameter, maximum circle equivalent bubble diameter in the horizontal plane, coordinates of the bubble centre of mass, moments characterizing asymmetries and others are obtained. Basing on the sphere equivalent bubble diameter cross-section and time-averaged bubble size distributions (Figs. 9–12) and radial gas volume fraction profiles decomposed according to the bubble size (Fig. 13) are calculated. The bubble size distributions are defined volume fraction related, i.e. they present the volume fraction per bubble diameter class: $\partial\alpha/\partial d_b \approx \Delta\alpha/\Delta d_b$. Integration over the bubble size distributions for this reason results in the time and cross-section averaged gas volume fraction.

Also for the bubble size distributions clear trends were observed. Fig. 9 gives an example for the evolution of the bubble size distributions with increasing L/D. Starting from the distribution measured close to the gas injection ($L/D = 1.1$) both coalescence (continuous increase of the largest bubbles measured) and fragmentation (continuous increase of the small bubble fraction peak) occur. The dependency of the distributions on the gas volume rate is demonstrated at Figs. 10 and 11. For small gas flow rates almost symmetrical distributions are obtained. They become more and

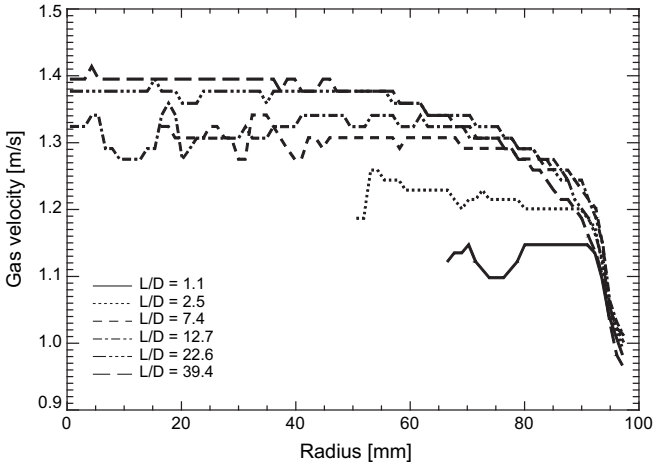

Fig. 7. Example for the evolution of the radial gas velocity profile with increasing distance between gas injection and measuring plane for a low void fraction case. $J_L = 1.017$ m/s, $J_G = 0.0062$ m/s, injection via 1 mm orifices.

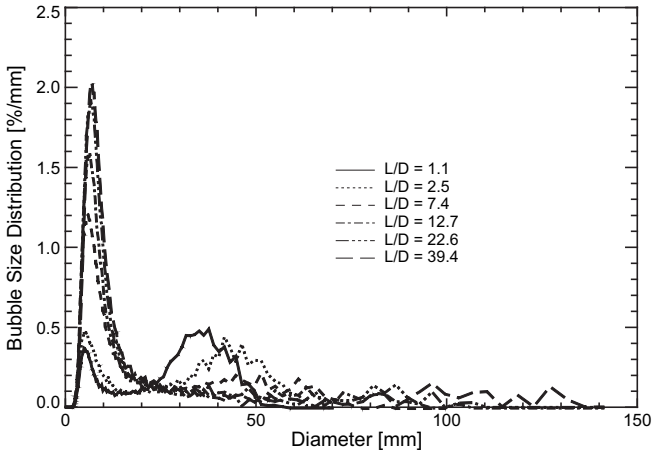

Fig. 9. Example for the evolution of bubble size distributions with increasing distance between gas injection and measuring plane. $J_L = 0.641$ m/s, $J_G = 0.219$ m/s, injection via 1 mm orifices.

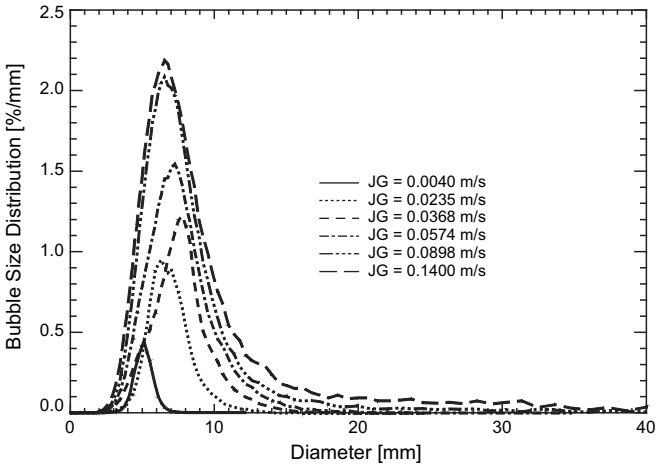

Fig. 10. Example for the dependency of bubble size distributions on the gas superficial velocity J_G in case of small void fractions. Liquid superficial velocity $J_L = 1.017$ m/s, injection via 1 mm orifices, $L/D = 39.9$.

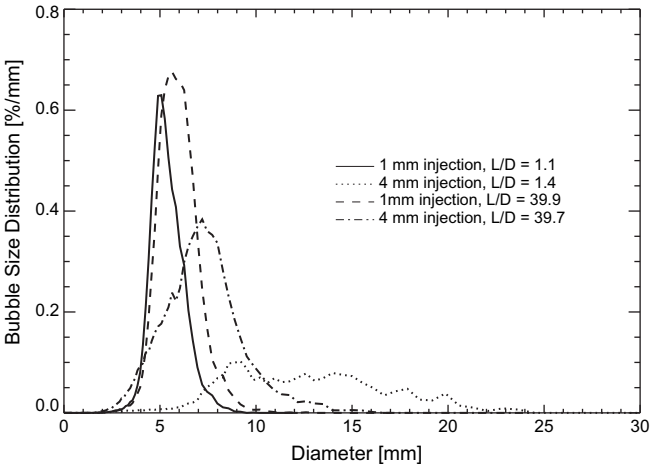

Fig. 12. Example for the dependency of the bubble size distributions on the type of injection orifices used. Liquid superficial velocity $J_L = 0.405$ m/s, gas superficial velocity $J_G = 0.0096$ m/s.

more pronounced on the right-hand side by an increase of J_G finally leading to bi-modal distributions as shown at Fig. 11. Fig. 12 demonstrates the influence of the injection orifices used which is important especially for cases with small void fraction.

The separation of small and large bubbles due to the lateral lift force mentioned above can clearly be shown by radial volume fraction profiles decomposed according to the bubble size as shown at Fig. 13. Tomiyama [25] proposed a correlation for the coefficient of the lateral lift force which depends on the bubble size basing on experiments on single bubbles. It predicts a change of the sign of this force at a sphere equivalent bubble diameter of 5.8 mm for our experimental conditions. Indeed, also for the poly-dispersed flow investigated here, bubbles smaller 5.8 mm sphere equivalent diameter form a clear wall peak while bubbles larger 7 mm are mainly found in the pipe centre.

4. Plausibility and accuracy of the data

4.1. Errors of boundary conditions and wire-mesh sensor measurements

All the standard instrumentation of the TOPFLOW facility as mass flow controllers or pressure transducer used are calibrated and have maximum errors in the order of 1%. Calibration protocols as well as the data regarding the accuracy for each single instrumentation are given in the experiment report by Beyer et al. [1].

To set a constant pressure at the gas injection (0.25 MPa (absolute)), the two-phase pressure drop in the test section was calculated to define the pressure boundary condition at the position of the pressure measurement (see Section 2.3). A constant drift velocity of 0.25 m/s was assumed for the calculation of the void fraction which influences the pressure drop. After completion of the experiments a "weighted drift velocity" was obtained (see Section 4.4) for each single measurement. This information was used to re-check the calculated set pressure values and to compare the results with the ones obtained for the assumed constant drift velocity. For most of the measurements the errors are clearly less than 1%, only in cases with high gas volume fractions (measuring matrix points 111–116, 127, 138, 149, 151, 160, 162, 171, 173, 182, 184, see Table 2) some larger errors up to 3.5% occur.

Errors of the wire-mesh sensor measurements for the gas fraction and bubble size are mainly caused by the interaction between bubbles and the wires. This results in general in a deceleration the bubbles. This effect is especially pronounced in case of small liquid velocities. The effect is small at liquid velocities larger ~ 0.2 m/s due to the momentum which pushed the bubbles through the

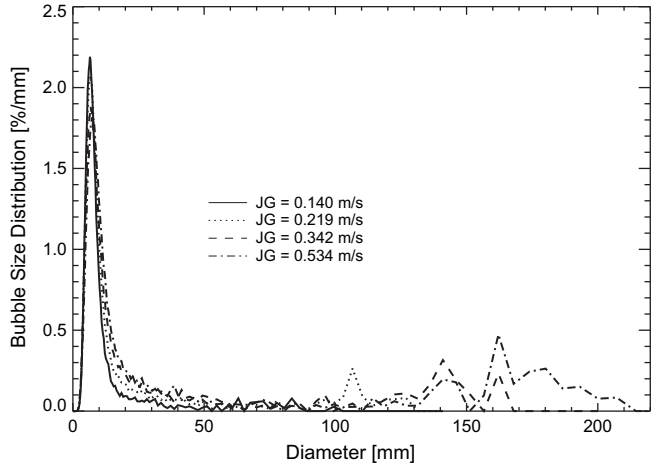

Fig. 11. Example for the dependency of bubble size distributions on the gas superficial velocity J_G in case of high void fractions. Liquid superficial velocity $J_L = 1.017$ m/s, injection via 1 mm orifices, $L/D = 39.9$.

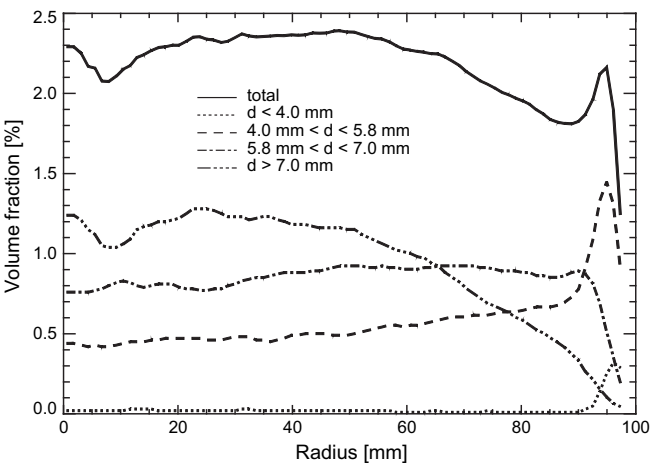

Fig. 13. Example for radial gas volume fraction profiles decomposed according to the bubble size. Liquid superficial velocity $J_L = 1.017$ m/s, gas superficial velocity $J_G = 0.0151$ m/s, injection via 1 mm orifices, $L/D = 39.9$.

sensor. Nevertheless the interaction of the flow with the wire-mesh sensor causes a systematic error which cannot be quantified directly. Instead comparisons with other measuring techniques are available as discussed below and checks on the gas volume flow rates reconstructed from the wire-mesh sensor measurements (Section 4.3) and on the cross-section and time-averaged gas volume fraction were done (Section 4.4).

Comparative measurements between the wire-mesh sensor and other research methods supplied information on the accuracy of the measurement technique and the evaluation algorithms for the experimental determination of these flow parameters. Gamma radiography of an air–water flow for varying superficial velocities of both media resulting in a gas volume fraction between 0 and 100% showed that the deviations between wire-mesh sensor and gamma measurement are limited to ±5% [14]. The radiography of a steam/water flow at atmospheric pressure confirmed this statement [9]. It has to be considered that the reference procedure has measurement errors, too. Comparative measurements between wire-mesh sensor and an X-ray tomography, which is a more exact reference procedure, were also done for air–water flow. As a result of this investigation it was found, that the accuracy of the gas volume fraction averaged over the flow cross-section depends on the two-phase flow regime. Differences in the absolute void fraction were determined [17] for a bubbly flow in the range of ±1% and for slug flow a systematic underestimation of approx. −4% was observed.

Comparative measurements with a high-speed camera are available to estimate the measurement error for the determination of the volume equivalent bubble diameter. The investigations were performed in a transparent flow channel where air–water flows with different bubble sizes. Prasser et al. [15] demonstrated that only bubbles with a diameter larger ∼ 2 mm can be recorded due to the limited spatial resolution in case of a wire-mesh sensor with a pitch of the wires of 3 × 3 mm. In addition, the comparisons between the data of the wire-mesh sensor and the high-speed camera showed that the volume equivalent diameter is measured at superficial water velocities of >0.2 m/s with an accuracy of ±20%. At smaller water velocities, overestimations up to +50% were observed. Note that the dispersion of the determined bubble sizes under constant flow conditions is significantly larger for the high-speed camera measurement than for the wire-mesh sensor. For this reason, it can be assumed that the indicated deviations between both procedures mainly results from the inaccuracy of the optical method.

The distance between the two measuring planes of the wire-mesh sensor used (40.5 mm) causes a discretization error for the gas velocity determined by the cross-correlation measurement of about 4% for the largest gas velocity (point 184) but is lower than 1% for all points of the measuring matrix ≤ 118.

4.2. Plausibility of the data

The radial profiles of the gas volume fraction and the gas velocity as well as the cross-section averaged bubble size distributions were plotted for all measuring points. Figs. 4–13 give some examples of such plots. A clear trend of the data with increasing L/D can be seen at these figures. There are no jumps or any inconsistency in the evolution of the curves. The plausibility and the evolution with increasing L/D were checked for all the measurements. In the result it was found, that the data fit very well to each other. For all data clear trends are observed and show a logical order. This is especially important for the use of the data to develop and validate models for bubble forces and bubble coalescence and fragmentation. A cross-check of the results of the different points of the measuring matrix was also done. Also for these checks the clear and plausible trends of the data can be confirmed.

4.3. Reconstructed gas volume flow rates

From the measured radial profiles of the void fraction and the velocity of the gas phase, the superficial gas velocity at the sensor can be calculated by integrating the product of both profiles over the pipe radius. Dependent on the test section height, the superficial gas velocity at the wire-mesh sensor can be obtained from the set values at the location of the active gas injection (i.e. at 0.25 MPa (a), see Table 1) by considering the Boyle–Mariotte's law. Fig. 14 compares the gas superficial velocities obtained from the measurement with the values obtained from the set values. In general there is a good agreement, but some systematic overestimation of the gas volume flow rate can be observed for low gas flow rates, independent on the size of the injection orifices used. It was found, that the relative overestimation for cases with small gas volume fractions, i.e. for cases with bubbly flow is at about 20%. This is not in conflict with the above mentioned comparisons with X-ray tomography since they were related to absolute errors.

Note that the deviations from the set value result from both the gas fraction and the velocity measurement. The reasons for the overestimation are presently under investigation. It can be assumed, that it is connected with the wire-mesh signals obtained in the case that the interface is between both layers of wires, i.e. also the vertical distance between the wires may play a role. A deceleration of the bubbles due to the contact with the wires was observed for low liquid velocities but should not be the reason for the deviations shown in Fig. 14 for $J_L = 1.017$ m/s. Nevertheless this effect is important in case of liquid superficial velocities below 0.4 m/s (points of the measuring matrix 034–038 and 111–115). For these points larger overestimations are observed. The results of this check are documented in detail in the experimental report by Beyer et al. [1].

4.4. Plausibility check for the integral gas volume fraction values

The aforementioned comparison of the gas superficial velocities obtained from the measurements with the set values always checks

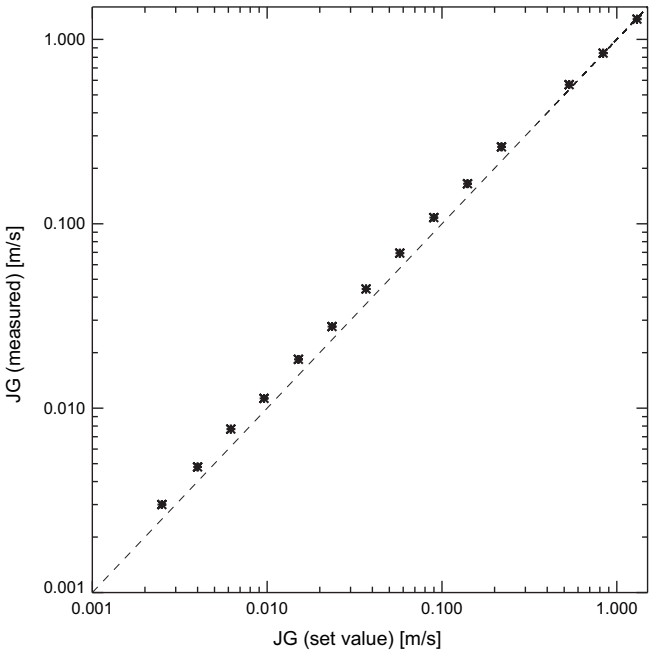

Fig. 14. Comparison of the superficial gas velocity J_G calculated from experimental data with the set values for $L/D = 39.9$, $J_L = 1.017$ m/s and injection via 1 mm orifices.

the gas volume fraction together with the gas velocity. An inaccuracy also arises from the fact, that only one velocity value is used for a given radial position of a bubble, i.e. the dependency of the bubble velocity on their size is neglected. In principle, this could be considered during the data evaluation, the statistical uncertainty, however, would be too high. For this reason here a mixed approach using correlations together with measured radial profiles and bubble size distributions is applied to check the plausibility of the measured values of the time and cross-section averaged gas volume fraction.

The gas volume fraction can be calculated from the superficial velocities of both phases J_L and J_G and the drift velocity U_D according to:

$$\varepsilon = \frac{J_G}{J_G + J_L + U_D}. \quad (1)$$

While J_L is the set value J_G has to be calculated from the set value at injection using the Boyle–Mariotte law due to the lower pressure at the measuring plane.

The drift velocity considering profile effects as well as the size dependent local bubble velocity can be calculated according to:

$$U_D = (C_0 - 1)J + U_{GJ}, \quad (2)$$

with the profile factor C_0 and the averaged local drift velocity U_{GJ}:

$$C_0 = \frac{2}{R^2\langle\varepsilon\rangle\langle j\rangle}\int_0^R j(r)\varepsilon(r)r\mathrm{d}r,$$

$$U_{GJ} = \frac{2}{R^2\langle\varepsilon\rangle}\int_0^R \sum_i (u_{D,i}\varepsilon_i(r))r\mathrm{d}r. \quad (3)$$

$\langle X\rangle$ stands for the cross-section averaged value of parameter X, $j(r)$ is the local superficial velocity, $\varepsilon_i(r)$ the gas volume fraction profile decomposed according to the bubble size class i, u_{Di} the local drift velocity of bubbles of class i and R is the pipe radius. The local drift velocity is calculated from a correlation for the terminal velocity of a bubble of size $d_{b,i}$ and a swarm correction. The complete procedure is described in the experimental report. It should be mentioned, that for the calculation of C_0 and U_{GJ} according to eq. (3) measured radial profiles are used, but they are normalized by their integral value what limits the influence of the measurement on the values obtained for the drift velocity.

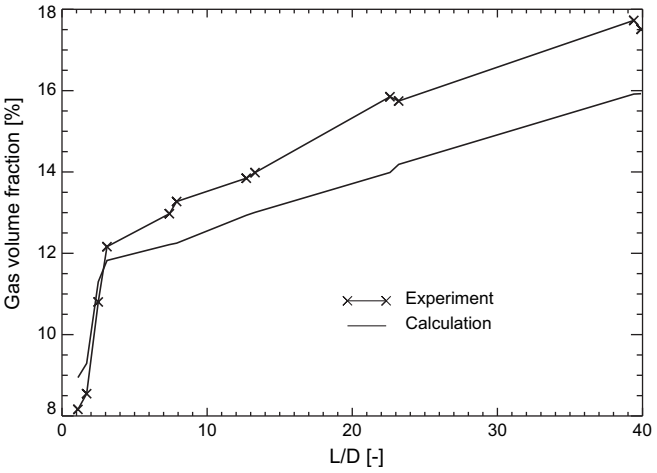

Fig. 16. Example for the dependency of the time and cross-section averaged gas volume fraction on the relative test section height L/D. The measured values are compared with values resulting from eqs. (1)–(3). $J_L = 0.405$ m/s, $J_G = 0.0898$ m/s, injection via 1 mm orifices.

Combining eqs. (1)–(3) slopes of the gas volume fraction in dependency on L/D can be calculated. Examples are shown in Figs. 15 and 16.

The measured integral gas volume fraction values and the calculated ones show the same trends. Nevertheless there is a systematic shift of the curves. This is an indication for a slight overestimation of the measured gas volume fraction. In general there is an increase of the void fraction due to decreasing pressure in the pipe. Close to the injection clear deviations from the approximately linear slope are observed. This different behaviour of the curves close to the injection results from profile effects. In case of low void fraction (Fig. 15) the profile of the liquid velocity remains nearly unchanged, i.e. the velocity of the gas injected from the wall is low (see Fig. 7). This low comparable low gas velocity causes the higher gas volume fraction values close to the gas injection, i.e. for small L/D. In case of higher gas flow rates, i.e. larger void fractions (Fig. 16) the liquid is accelerated in the wall region by the injected bubbles and secondary flows occur (compare also Fig. 8). This causes higher gas velocities and thus lower void fraction values in the vicinity of the injection.

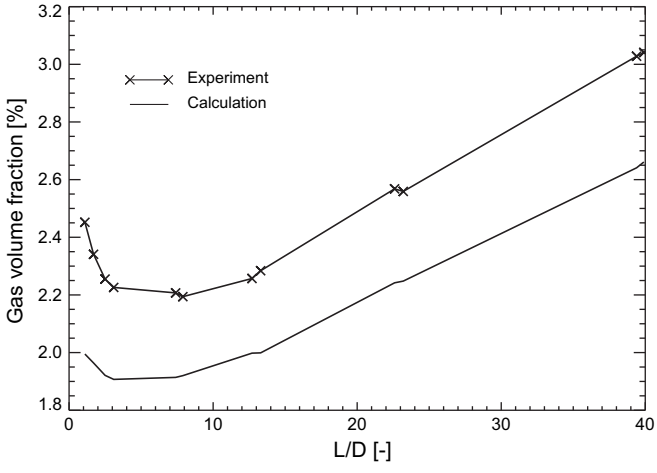

Fig. 15. Example for the dependency of the time and cross-section averaged gas volume fraction on the relative test section height L/D. The measured values are compared with values resulting from eqs. (1)–(3). $J_L = 1.017$ m/s, $J_G = 0.0235$ m/s, injection via 1 mm orifices.

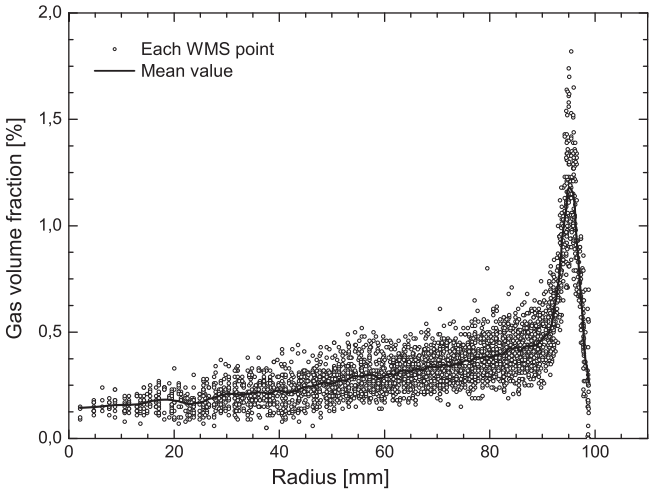

Fig. 17. Example for scattering of temporal averaged gas volume fraction values of each WMS crossing point. $J_L = 1.017$ m/s, $J_G = 0.0025$ m/s, $L/D = 39.9$.

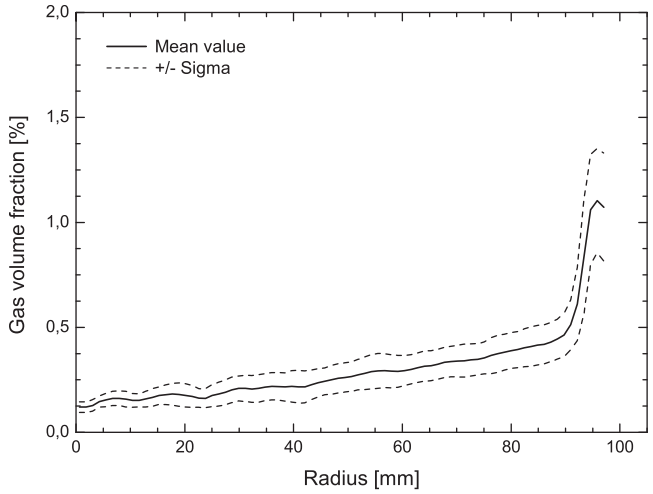

Fig. 18. Temporal and azimuthally averaged gas volume fraction profile with standard deviation lines. $J_L = 1.017$ m/s, $J_G = 0.0025$ m/s, $L/D = 39.9$.

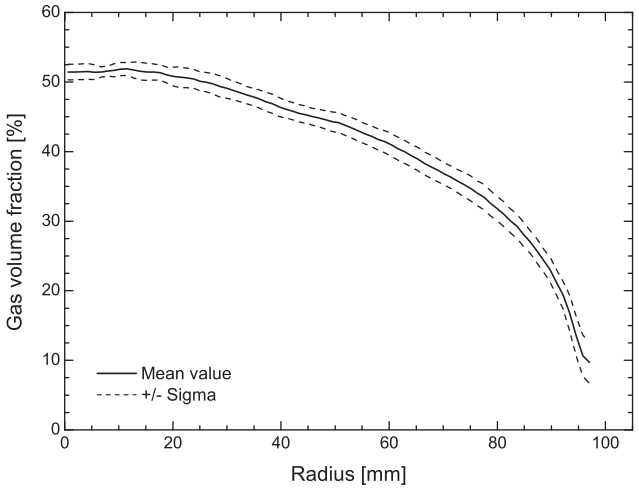

Fig. 20. Temporal and azimuthally averaged gas volume fraction profile with standard deviation lines. $J_L = 1.017$ m/s, $J_G = 0.534$ m/s, $L/D = 39.9$.

4.5. Statistical error of the radial gas volume fraction profiles

As mentioned above systematic errors caused by the wire-mesh sensor technique have to be considered. The comparisons and checks of integral values presented above enable a global error assessment, but no quantitative values like error bars for the presented radial profiles or bubble size distributions can be obtained. In addition to this systematic error also statistical errors occur. Due to the high number of bubbles which cross the sensor during the measuring time, these errors are rather small for time-averaged properties.

As mentioned above the radial gas volume fraction profiles are obtained by an azimuthally averaging over the values from the single crossing points of the wires. The scatter of single values can be used to determine error bars for the radial profiles of the gas volume fraction.

Examples for time-averaged gas volume fraction values for each single crossing point of the wires are presented in Fig. 17 for the lowest gas superficial velocity and in Fig. 19 for a higher one. In addition to these values there is also a line displayed which represents the mean value of crossing points with the same radius.

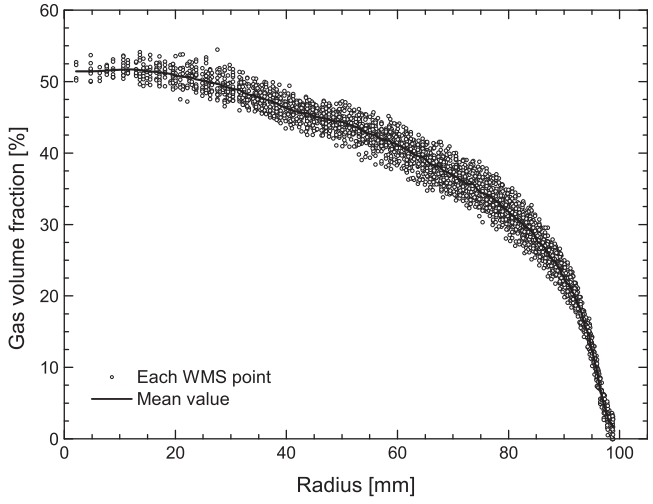

Fig. 19. Example for scattering of temporal averaged gas volume fraction values of each WMS crossing point. $J_L = 1.017$ m/s, $J_G = 0.534$ m/s, $L/D = 39.9$.

As discussed above the radial gas volume fraction profiles result from an averaging which considers the contribution of each single crossing point to 80 ring-shaped domains. For analyzing the statistical error of these values, standard deviations of these 80 mean values are determined. Figs. 18 and 20 are showing examples for gas volume fraction profiles together with their standard deviation. The scattering to smaller and larger values was considered separately resulting in a lower and upper error bound.

Such error bounds were calculated for all test matrix points. In most cases it is visible that the scattering is lower at the pipe centre as the pipe wall. The segmentation of circular cross-section of the wire-mesh sensor into ring-shaped domains entails a different number of crossing points per domain, so the statistics becomes better with increasing radius. It has to be considered, that less than 10 crossing points contribute to the 3 inner domains. This limits the significance of the obtained standard deviations for these domains.

Another effect was observed at lower gas superficial velocities. By using the 4 mm gas injection orifices the scattering of gas volume fraction values is higher then by using the 1 mm orifices, because the 1 mm injection unit produces smaller bubbles which are more homogeneous distributed in the two-phase flow. This effect disappears at higher gas superficial velocities.

5. Conclusions

A new detailed database on air–water flow in a vertical pipe with an inner diameter of 195.3 mm for a wide range of flow rates was established. It includes detailed information on the evolution of the flow along the pipe and closes a gap which exists for data suitable for the development and validation of models for bubble coalescence and break-up. It is clearly distinguished for their quality and their extensiveness. The variable gas injection was used to vary the distance between gas injection and measuring plane. Although in this case the gas is injected via orifices in the pipe wall from injection chambers which are located at different height positions at the pipe the experimental data exactly reflect the situation of a gas injection at a fixed position and a shifting of the measuring plane. This was achieved by setting the pressure at the height of the activated gas injection to a fixed value of 0.25 MPa (absolute).

Measurements were done using the wire-mesh sensor technology. A double sensor with 64 × 64 wires for each measuring plane was used. A single measurement last 10 s, the measuring

frequency is 2500 frames per second. From the three-dimensional matrix of local instantaneous gas volume fraction values time-averaged profiles and distributions are obtained which are suitable for model development and validation. Among these data are radial profiles of the void fraction and the gas velocity as well as bubble size distributions. Also double-differential void fraction data regarding radial position and bubble size were obtained.

Extensive checks were done regarding the data quality. It was found, that the consistency of the data to each other is excellent, while a slight overestimation of the measured integral gas volume fraction has to be considered. Nevertheless the data in their detailedness are unique world-wide and probably have the best quality. A detailed documentation of the experiments and the quality checks is given by Beyer et al. [1]. The database is a suitable test case for the simulation of poly-dispersed bubbly flows. This includes the development, test and validation of closure models, e.g. for bubble forces and for bubble coalescence and fragmentation.

Acknowledgements

This work is carried out in the frame of a current research project funded by the German Federal Ministry of Economics and Labour, project number 150 1329. The authors like to thank all members of the TOPFLOW team who contributed to the successful performance of these experiments.

References

[1] M. Beyer, D. Lucas, J. Kussin, P. Schütz, Air–water experiments in a vertical DN200-pipe, Report FZD-505, 2008.
[2] H. Chang, J.H. Hills, B.J. Azzopardi, A study of the bubble-to-slug transition in vertical gas–liquid flow in columns of different diameter. International Journal of Multiphase Flow 24 (1998) 431–452.
[3] T. Hibiki, M. Ishii, Experimental study on interfacial area transport in bubbly two-phase flows. International Journal of Heat and Mass Transfer 42 (1999) 3019–3035.
[4] R. Kaji, B.J. Azzopardi, D. Lucas, Investigation of flow development of co-current gas–liquid vertical slug flow. International Journal of Multiphase Flow 35 (2009) 335–348.
[5] E. Krepper, D. Lucas, T. Frank, H.-M. Prasser, P. Zwart, The inhomogeneous MUSIG model for the simulation of polydispersed flows. Nuclear Engineering and Design 238 (2008) 1690–1702.
[6] D. Lucas, E. Krepper, H.-M. Prasser, Development of co-current air–water flow in a vertical pipe. International Journal of Multiphase Flow 31 (2005) 1304–1328.
[7] D. Lucas, E. Krepper, H.-M. Prasser, Modelling of the evolution of bubbly flow along a large vertical pipe. Nuclear Technology 158 (2007) 291–303.
[8] D. Lucas, E. Krepper, H.-M. Prasser, Use of models for lift, wall and turbulent dispersion forces acting on bubbles for poly-disperse flows. Chemical Science and Engineering 62 (2007) 4146–4157.
[9] A. Manera, H.-M. Prasser, T.H.J.J. Van der Hagen, R.F. Mudde, J.M. de Kruijf, A comparison of void-fraction measurements during flashing-induced instabilities obtained with a wire-mesh sensor and a gamma-transmission set-up, in: 4th International Conference on Multiphase Flow, New Orleans, USA, Paper No. 436, 2001.
[10] A. Manera, B. Ozar, S. Paranjape, M. Ishii, H.-M. Prasser, Comparison between wire-mesh sensors and conductive needle-probes for measurements of two-phase flow parameters. Nuclear Engineering and Design 239 (2009) 1718–1724.
[11] M. Misawa, A. Suzuki, Y. Morikawa, A. Minato, H.-M. Prasser, Nonlinear characteristics of gas–liquid two-phase flow and verification of extended two-fluid model, in: 5th International Conference on Multiphase Flow, ICMF'04, Yokohama, Japan, Paper No. 213, 2004.
[12] A. Ohnuki, H. Akimoto, Experimental study on transition of flow pattern and phase distribution in upward air–water two-phase flow along a large vertical pipe. International Journal of Multiphase Flow 26 (2000) 376–386.
[13] H.-M. Prasser, A. Böttger, J. Zschau, A new electrode-mesh tomograph for gas/liquid flows. Flow Measurement and Instrumentation 9 (1998) 111–119.
[14] H.-M. Prasser, High-speed measurement of the void fraction distribution in ducts by wire-mesh sensors, in: International Meeting on Reactor Noise, Athen, 2000.
[15] H.-M. Prasser, D. Scholz, C. Zippe, Bubble size measurement using wire-mesh sensors. Flow Measurement and Instrumentation 12 (2001) 299–312.
[16] H.-M. Prasser, E. Krepper, D. Lucas, Evolution of the two-phase flow in a vertical tube – decomposition of gas fraction profiles according to bubble size classes using wire-mesh sensors. International Journal of Thermal Sciences 41 (2002) 17–28.
[17] H.-M. Prasser, M. Misawa, I. Tiseanu, Comparison between wire-mesh sensor and ultra-fast X-ray tomograph for an air/water flow in a vertical pipe. Flow Measurement and Instrumentation 16 (2005) 73–83.
[18] H.-M. Prasser, M. Beyer, H. Carl, A. Manera, H. Pietruske, P. Schütz, F.-P. Weiß, The multipurpose thermal–hydraulic test facility TOPFLOW: an overview on experimental capabilities, instrumentation and results. Kerntechnik 71 (2006) 163–173.
[19] H.-M. Prasser, M. Beyer, H. Carl, A. Manera, H. Pietruske, P. Schütz, Experiments on Upwards Gas/Liquid Flow in Vertical Pipes (2007) Report FZD-482 Available online at: http://www.fzd.de/publications/010475/10475.pdf.
[20] H.-M. Prasser, M. Beyer, H. Carl, S. Gregor, D. Lucas, H. Pietruske, P. Schütz, F.-P. Weiss, Evolution of the structure of a gas–liquid two-phase flow in a large vertical pipe. Nuclear Engineering and Design 237 (2007) 1848–1861.
[21] A. Schaffrath, A.-K. Krüssenberg, F.-P. Weiß, E.-F. Hicken, M. Beyer, H. Carl, H.-M. Prasser, J. Schuster, P. Schütz, M. Tamme, TOPFLOW – a new multipurpose thermalhydraulic test facility for the investigation of steady state and transient two-phase flow phenomena. Kerntechnik 66 (2001) 209–212.
[22] K. Sekoguchi, K. Mori, New development of experimental study on interfacial structure in gas–liquid two-phase flow, in: 4th International Conference on Experimental Heat Transfer, Fluid Mechanics and Thermodynamics, Brussels, Belgium, Proceedings, vol. 2, pp. 1177–1188, 1997.
[23] X. Shen, K. Mishima, H. Nakamura, Two-phase phase distribution in a vertical large diameter pipe. International Journal of Heat and Mass Transfer 48 (2005) 211–225.
[24] X. Sun, T. Smith, S. Kim, M. Ishii, J. Uhle, Interfacial area of bubbly flow in a relatively large diameter pipe. Experimental Thermal and Fluid Science 27 (2002) 97–109.
[25] A. Tomiyama, . Struggle with computational bubble dynamics, in: 3rd International Conference on Multiphase Flow, ICMF'98, Lyon, France, 1998.
[26] K. Yoneda, A. Yasuo, T. Okawa, S.-R. Zhou, Flow structure of developing steam-water two-phase flow in a large-diameter pipe, in: Proceedings of ICONE 8, 8th International Conference on Nuclear Engineering, Baltimore, MD, USA, Paper ICONE-8330, 2000.